Synthesis, growth, structural, physicochemical, linear and nonlinear optical properties of new hybrid [(Ba(C$_{10}$H$_{20}$O$_5$)$_2$)· (Mn (SCN)$_4$)] single crystal

V. Ravisankar[1] · V. Ramesh[1] · T. C. Sabari Girisun[2] · D. V. Sridevi[3] · B. Gunasekaran[1]

Abstract

A novel nonlinear optical single crystal of barium (II) 15-crown-5-ether manganese (II)-tetra-thiocyanate (Ba(C$_{10}$H$_{20}$O$_5$)$_2$)· (Mn(SCN)$_4$); (BBCMTC) has been grown in a period of 15–20 days by slow evaporation solvent technique with the dimension of $10 \times 5 \times 2$ mm^3. Single crystal X-ray diffraction shows BBCMTC crystallizes in orthorhombic crystal system with space group Pnma. In Powder X-Ray diffraction, the *hkl* plane orientations reveal the phase identification of the grown crystal. The estimated lattice parameters ($a = 15.9102$ Å, $b = 12.6164$ Å, $c = 18.3959$ Å, $\alpha = \beta = \gamma = 90°$ and $V = 3696.26$ Å^3) are well-matched in both powder and single crystal XRD. Spectroscopic analysis of FTIR and micro-Raman confirmed the existence of C–N stretching of SCN, C–C stretching of ring, metal–nitrogen bonding and Ba–O groups. BBCMTC possess lower cut-off wavelength of 287 nm and wide optical band gap of 4.1 eV. FE-SEM and optical microscopic studies revealed the presence of voids on the surface of grown crystal and reverse growth rate facets. TG–DTA and DSC measurements revealed that the crystalline compound has better thermal stability (382 °C) than other inorganic–organic crystalline compounds such as CLTC (171 °C) and ACCTC (247 °C). Vickers's hardness test shows the material belongs to soft materials category ($n = 3$). Variation of dielectric constant and dielectric loss with frequency and temperature was analyzed. Furthermore, dielectric solid-state parameters such as valence electron plasma energy ($\hbar \omega_P$), Penn gap (E_P), Fermi energy (E_F), and electronic polarizability (α) were calculated. The third-order nonlinear optical coefficients such as nonlinear refractive index ($n_2 = 7.86 \times 10^{-8}$ cm^{2}W^{-1}), nonlinear absorption coefficient ($\beta = 4.50 \times 10^{-3}$ cmW^{-1}) and nonlinear optical susceptibility ($\chi^3 = 11.55 \times 10^{-5}$ esu) obtained from *Z*-scan studies under 785 nm excitation. Therefore, BBCMTC single crystal with higher thermal stability and third-order NLO coefficient finds potential applications in optoelectronics and optical switching device fabrications.

Keywords Single crystal · XRD · Spectroscopic · TG-DSC · Etching · Vickers's hardness measurement · And *Z*-scan studies

1 Introduction

Metal–organic nonlinear optical (NLO) crystalline materials finds potential applications in optoelectronic devices. Among them hybrid metal–organic thiocyanate crystalline compounds that combines thiocyanate (SCN)⁻ complex crystal with inorganic elements possess interesting optical properties [1–5]. Additionally, these class of crystals has excellent thermal stability and better mechanical strength. Growing high-quality NLO materials is a fundamental building block for great attention as single crystals are in much demand for efficient frequency conversion, laser spectroscopy, optical switching, optical storage, information processing, computing, and optical bi-stable device [6–11]. The bimetallic complex thiocyanate series that is

✉ B. Gunasekaran
gunasekb@srmist.edu.in; phdguna@gamil.com

1 Department of Physics and Nanotechonolgy, SRM Institute of Science and Technology, Kattankulathur, Tamil Nadu 603 203, India

2 Nanophotonics Laboratory, School of Physics, Bharathidasan University, Tiruchirappalli, Tamil Nadu 620 024, India

3 Department of Chemistry, Rajalakshmi Institute of Technology, Kuthambakkam, Chennai 600124, India

found to crystallize in centrosymmetric space group with general formula $AB(SCN)_4$ (A-alkali earth metals Ba^{2+}, Mg^{2+}), (B-transition metals Zn^{2+}, Mn^{2+}, Fe^{2+}, Ni^{2+} Hg^{2+}, etc.) exhibit polymeric structure with a three-dimensional ($-S=C=N-$) network [12, 13]. An essential characteristic of crown ether selectivity (hosts) and their metal complexes (guests) to form these classes depends on the radius of the cavity, and the size of the cation. According to atomic models, Pederson estimated the radius value of 15-Crown-5-ether to be 1.7–2.2 Å [14]. The crown ether with or without oxygen (O), nitrogen (N), and sulphur (S) atoms have been found to possess higher-order nonlinear optical properties [15]. Ligands that receive the thiocyanate's conjugated bonding electron and interact with two metal ions *A* and *B* have continuously connected to a big alkali-metal ions Ba (2.68 Å) thiocyanate of the sulphur site. In contrast, the small bivalent metal ions Mn (2.17 Å) have bonded to nitrogen end and to form the new combination of $(Ba(C_{10}H_{20}O_5)_2)$ $(Mn (SCN)_4)$. The transition metals and the ligand building block network are the backbone for forming the SCN ligand, and low energy *d-d* transition that happens in all organometallic combinations has been identified in the visible light region [16].

A new series of an inorganic–organic single crystal of $Ba(C_{10}H_{20}O_5)_2)$ $(Mn(SCN)_4)$ [BBCMTC] was synthesized from aqueous solutions via slow evaporation solvent technique. The grown single crystal structure was confirmed by single crystal X-ray diffraction analysis, and the crystal structure was deposited in the Cambridge Crystallographic Data Centre (CCDC No: 1966145). The spectroscopic characterization of BBCMTC such as FT-IR, micro- Raman, UV–Vis-NIR, and EDAX was measured systematically. The surface morphology, reverse growth rate has been observed by FE-SEM, optical microscope, and Vickers's hardness measurements. Furthermore, the third-order nonlinear optical properties were calculated by *Z*-scan technique using a continuous wave laser with wavelength of 785 nm. The grown crown ether and thiocyanate derivatives exhibit high thermal and mechanical stability, making them appropriate for optical device applications.

2 Experimental sections

2.1 Material synthesis and growth

The slow evaporation solution growth technique (SESGT) was employed to grow single crystals of BBCMTC. Initially, all the synthesis chemicals were purchased with AR grade. The commonly available barium chloride ($BaCl_2$) of 99% purity, manganese chloride ($MnCl_2$) of 99% purity, 15-crown-5-ether ($C_{10}H_{20}O_5$) of 98% purity and ammonium thiocyanate (NH_4SCN) of 97% purity was purchased and

used without any further purification. The above mentioned precursors were taken in the stoichiometric ratio of 1:1:2:4 and then dissolved in mixed solvent of methanol with water taken in the stoichiometric ratio of 1:1.

$$BaCl_2 + MnCl_2 + 2(C_{10}H_{20}O_5) + 4[NH_4SCN]$$
$$\rightarrow [2(C_{10}H_{20}O_5) Ba] \cdot Mn (SCN_4) + 4NH_4Cl$$
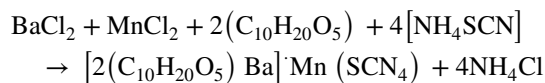
Employing the above reaction scheme, the starting chemicals of $BaCl_2$, $MnCl_2$, and $NH_4(SCN)$ were dissolved in double deionized water and taken in different beakers. All these three chemical compounds were added and stirred for 1 h to get a clear solution. The inorganic chemical compound of 15-crown-5ether ($C_{10}H_{20}O_5$) solution was added with the mixed solution in drop-wise manner and then the solutions were vigorously stirred for 8 h. Finally, a small amount of precipitate formed was gently heated above room temperature (maximum + 5 °C) to increase the solubility of the solution. Finally, the pale-yellow colored solution we collected. The saturated homogeneous solution was filtered with Whatman filter paper and allowed to SESGT. A good optical grade pale-yellow colored crystal of dimension $10 \times 5 \times 2$ mm^3 was harvested over a period of 15–20 days and is as shown in Fig. 1.

3 Results and discussions

3.1 Crystal structural studies: single crystal and powder XRD

Bruker- Kappa APEX II CCD diffractometer with Molybdenum Kα radiation has been used to collect the SXRD
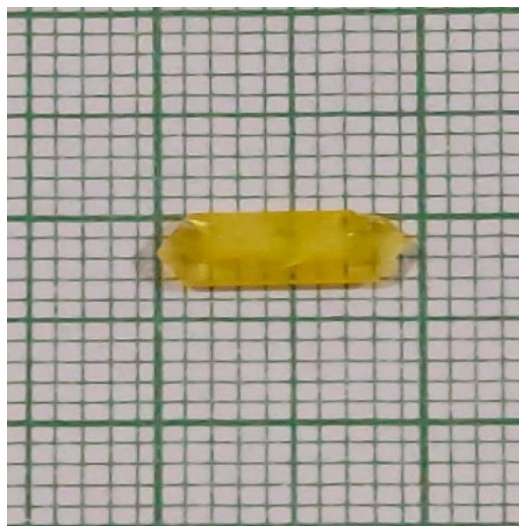

Fig. 1 Photograph of BBCMTC single crystal

data. The unit cell parameters and orientation matrix are obtained between the reflections range 3.56° and 24.99° [17]. The total number of reflections collected was 75,021, out of which 3390 were independent reflections and 3181 are $I > 2\sigma(I)$. SADABS [18] was used to correct Lorentz and polarization effects. The SHELXS97 [19] program was used to solve the crystal structure of the title compound and refined by SHELXL2018 [20]. All the non-hydrogen atoms were included in the respective position by using full-matrix least square refinement and the final R-factor was 0.0447. The crystallographic data (CCDC: 1,966,145) of the title compound were summarized in Table 1. The title compound crystallizes in the orthorhombic system with space group Pnma and it mimics the orthorhombic crystal system of other thiocyanate crystal family such as MMTD, MMTG, CMTD, MMTN and CMTG [21–23]. Figure 2a shows the 30% probability ellipsoid ORTEP plot of the title molecule. The grown crystal consists of Ba^{II} and Mn^{II} ions and both the ions are surrounded by twofold rotational axes. The asymmetric unit consists of half each of the complex cations and anions. The Mn^{II} is surrounded by four N atoms and Ba^{II} ion is coordinated by 10 O atoms from two 15-crown-5 ligand in a sandwich-like configuration. In the title molecule, both the 15-crown-5 ligands are disordered over two positions. The site occupancy factors of disordered carbon and oxygen atoms, respectively, C1, C2, C3, C4, C5, O1, O2 and O3 was redefined as 0.588 (7) during anisotropic refinement and the same of C1′, C2′, C3′, C4′, C5′, O1′, O2′ and O3′ was redefined as 0.412 (7) during anisotropic refinement. Similarly, the site occupancy of atoms C6, C7, C8, C9, C10, O4, O5 and O6 was redefined as 0.704 (7) and the same of C6′, C7′, C8′, C9′, C10′, O4′, O5′ and O6′ was redefied as 0.296 (7) during the anisotropic refinement using SIMU and SADI command in SHELXL2018 [24] with an effective deviation of 0.02. The Ba–O and Mn–N bond lengths are comparable with those observed in other similar complex structures [25–27]. The molecular packing of the title compound is stabilized by weak C–H…S intermolecular

Table 1 Crystal data, data collection and structure refinement

| Identification code	Shelx	
Empirical formula	C24 H40 Ba Mn N4 O10 S4	
Formula weight	865.12	
Temperature	296(2) K	
Wavelength	0.71073 Å	
Crystal system	Orthorhombic	
Space group	P n m a	
Unit cell dimensions	$a = 15.9102(15)$ Å	$\alpha = 90°$
	$b = 12.6164(12)$ Å	$\beta = 90°$
	$c = 18.3959(18)$ Å	$\gamma = 90°$
Volume	3692.6(6) Å^3	
Z	4	
Density (calculated)	1.556 Mg/m^3	
Absorption coefficient	1.679 mm^{-1}	
F(000)	1748	
Crystal size	$0.200 \times 0.200 \times 0.150$ mm^3	
Theta range for data collection	3.561–24.995°	
Index ranges	$-18 <= h <= 18, -15 <= k <= 15, -21 <= l <= 21$	
Reflections collected	75,021	
Independent reflections	3390 [R(int) = 0.0509]	
Completeness to theta = 24.995°	99.4%	
Absorption correction	Semi-empirical from equivalents	
Max. and min. transmission	0.7454 and 0.6766	
Refinementmethod	Full-matrix least-squares on F^2	
Data/restraints/parameters	3390/493/349	
Goodness-of-fit on F^2	1.029	
Final R indices [$I > 2$sigma(I)]	R1 = 0.0419, wR2 = 0.1128	
R indices (all data)	R1 = 0.0447, wR2 = 0.1170	
Extinction coefficient	0.0065(7)	
Largest diff. peak and hole	0.774 and -0.793 e.Å^{-3}	

(a)

(b)
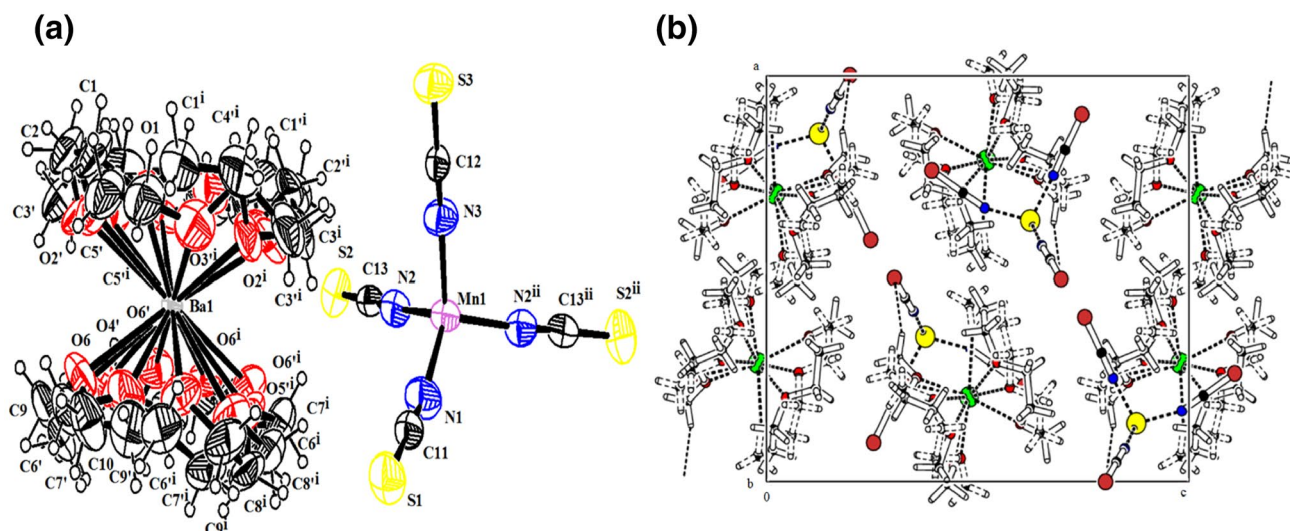
Fig. 2 **a** ORTEP plot of the molecule with atom numbering scheme drawn at 30% probability ellipsoid level. **b** The packing of the title compound, viewed down the b axis. Hydrogen bonds are shown as dashed lines

Table 2 Hydrogen bond data and angle (Å and °) of the compound

D–H…A	D–H	H…A	D…A	DHA
C2–H2B…S2^i^	0.97	2.95	3.90 (3)	166.8 3_556
C5–H5A…S2^ii^	0.97	2.73	3.630 (14)	154.9 8_565
C8–H8B…S1^iii^	0.97	3.02	3.817 (13)	140.3 1_545
C10–H10A…S3^iv^	0.97	2.91	3.704 (13)	139.3 5_766

Symmetry Elements: (i) $x+1/2, -y+1/2, -z+3/2$ (ii) $x, -y+1/2, z$ (iii) $x, y-1, z$ (iv) $-x+2, -y+1, -iz+1$

hydrogen bond. Table 2 gives the Hydrogen bond data of the compound. Figure 2b shows the C–H…S interaction of the title compound. In addition to the SXRD, further verification of lattice parameters were made by PXRD studies. The powder form sample was tested in PAN ANALYTICAL diffractometer with CuKα radiation ($\lambda = 1.5405$ Å) over a 2θ angle between 10° and 50° with a scanning speed of 25 min. All the diffraction peaks were indexed by using Vesta software (open GL version: 3.1.0-Build 9.17.10.4459) and is shown Fig. 3. The strongest reflection at 10.19° represents the (111) crystal face and sharpness of peaks in PXRD displays the high crystallinity of BBMCTC. The various crystal planes are listed in Table 3 and the lattice cell parameters of the title compound $a = 15.9102$ Å, $b = 12.6164$ Å, $c = 18.3959$ Å and $V = 3696.59$ Å^3 were well-matched with the SXRD data [28, 29].

3.2 UV–Vis-NIR spectral analysis

The optical absorbance and transmissions of grown single crystal of BBCMTC were examined by UV–Vis-NIR
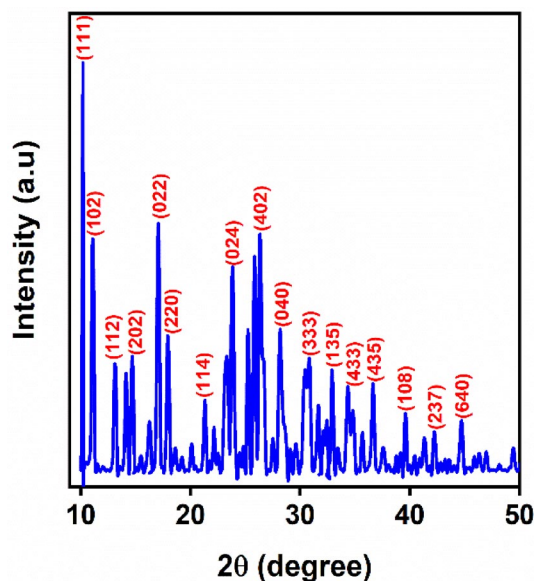

Fig. 3 PXRD profile of BBCMTC

spectrum with the ranges from 200 to 2000 nm. The recorded absorbance and transmittance spectrum are shown in Fig. 4a, b. The lower cut-off wavelength of the BBCMTC crystal was observed at 287 nm and it matches with the other thiocyanate family crystals (ZCTC-290 nm, TCTZ-290 nm, ZMTC-260 nm and, MCCTC-277 nm) [30–33]. Further the crystal exhibits high transmittance in the visible and NIR region with wide optical window of 400–2000 nm. The optical properties like optical bandgap (E_g) and optical absorption coefficient (α) are depend on optical transmittance of organometallic thiocyanate crystal. The optical

Table 3 As selected PXRD spectral data of BBCMTC

| Peak no	h k l	d (Å)	F (real)	|F|	2θ	Intensity
1	1 1 1	8.707	−242.418	243.68	10.174	49.745
2	1 0 2	7.963	124.337	125.235	11.102	11.015
3	1 1 2	6.733	−82.586	82.983	13.168	3.4227
4	2 0 2	6.016	−178.48	181.191	14.710	1.0280
5	0 2 2	5.202	−189.823	192.576	17.071	16.232
6	2 2 0	4.942	245.261	247.651	17.931	11.040
7	1 1 4	4.169	−144.890	145.021	21.343	3.8843
8	0 2 4	3.716	−214.504	215.216	23.984	3.3531
9	4 0 2	3.650	−17.3905	22.085	24.361	0.0683
10	0 4 0	3.154	322.590	325.409	28.341	2.6943
11	3 3 3	2.902	−192.607	193.449	30.779	6.3849
12	1 3 5	2.7280	200.872	203.14	32.884	3.0519
13	4 3 5	2.2725	−61.191	61.375	39.626	0.3700
14	1 0 8	2.2758	155.823	157.917	39.666	0.6111
15	2 3 7	2.1460	70.552	73.553	42.177	0.2312
16	6 4 0	2.0297	32.563	32.672	44.720	0.0200
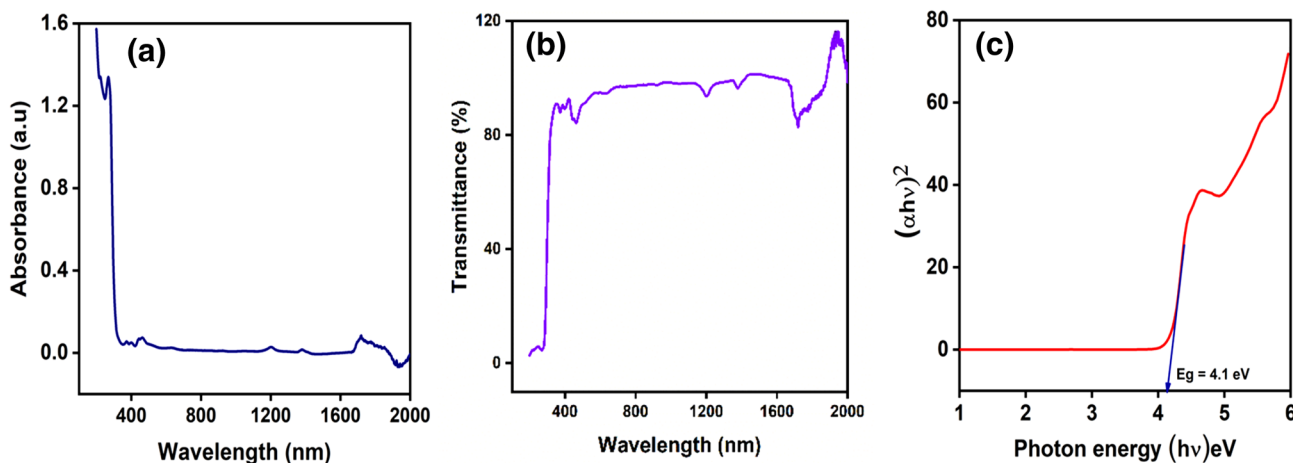
Fig. 4 **a** UV–Vis-NIR absorbance spectrum, **b** Transmission spectrum, **c** Optical bandgap spectrum

absorption coefficient (α) was calculated with the following relation [34–37]

$$\alpha = \frac{2.3026}{t} \log_{10}\left(\frac{100}{T}\right) \tag{1}$$

where 't' and 'T' are the thickness and transmittance (%) of the crystal.

The optical bandgap (E_g) was estimated from the absorption coefficient (α) near the absorption edge using the formula.

$$\alpha h\gamma = A\left(h\gamma - E_g\right)^2 \tag{2}$$

where 'A' is constant, 'h' is Planck's constant (6.626×10^{-34} J/s) and 'E_g' is the optical energy bandgap.

Tauc's plot between $(\alpha h\gamma)^2$ versus photon energy ($h\gamma$). Plotted Tauc's plot is shown in Fig. 4c, and the optical bandgap was found as 4.1 eV.

Additionally, the optical band gap energy (E_g) was also calculated using theoretical relation

$$E_g = \frac{1240}{\lambda} \text{eV} \tag{3}$$

where 'λ' is the lower cut-off wavelength (287 nm). The optical bandgap of grown BBCMTC single crystal value was calculated to be 4.3 eV. Closeness in the experimental and theoretical values of optical band gap exposes the good crystalline nature of the grown crystal. Further the optical band gap of BBCMTC falls at the similar wide band gap domain of other thiocyanate crystal of MCCTC (4.33 eV) [33].

Lower cut-off wavelength and wide optical transmittance makes the grown crystal suitable for NLO applications.

3.3 FTIR and micro-Raman spectral analysis

Fourier transform infrared (FT-IR) and Raman spectroscopy studies were performed to confirm the presence of functional groups and the molecular structure of the title compound. FTIR was recorded with BRUKER IFS—66 V FTIR spectrometer using KBr pellet method (10:1) in the wavenumber region of 400–4000 cm^{-1}. The title crystal transmittance spectra is shown in Fig. 5a and the corresponding spectral assignments observed are presented in the Table 4. The peak from 3967 to 3432 cm^{-1} represents O–H stretching vibrations. The higher wavenumber region 2878–2926 cm^{-1} is observed due to C–H stretching vibrations. The C–N stretching vibration of SCN of the thiocyanate group appear as a sharp intensity band appeared at 2041 cm^{-1} and 1248 cm^{-1} [5, 10]. The peak occurring at 1470 cm^{-1} is due to C–C stretch (in ring) or C–H bend. The peak position at 1357 cm^{-1} arises from C–H rocking vibrations. The peaks at 1300 cm^{-1} and at 944 cm^{-1} is assigned to C–H wagging and = C–H bending vibrations. The metal–nitrogen stretching vibrations was observed at 574 cm^{-1}. Additionally, Raman spectra of title crystal was recorded in the wavenumber range of 0–4000 cm^{-1} at room temperature. The Raman spectrum of BBCMTC crystal also confirms the stretching vibration of SCN by the peak at 2054 cm^{-1} as shown in Fig. 5b [3, 38]. Also the C–H stretching vibrations were observed at 2929 cm^{-1} and 2880 cm^{-1}. The metal–nitrogen vibration observed in IR at 574 cm^{-1} appears at 559 cm^{-1} in Raman spectra. Further the lattice vibration mode in the lower frequency range 284 cm^{-1}, 136 cm^{-1} and 70 cm^{-1} are

Table 4 Various functional group assignments for FTIR and micro-Raman for BBCMTC crystal

Wave number (cm^{-1})		Band assignments
IR	Raman	
3967–3432	–	O–H stretching vibrations
2926 &2878	2929 &2830	C–H stretching vibrations for alkanes
2041	2054	CN-stretching vibration SCN of (thiocyanate)
1470	–	C–C stretch (in ring) or C–H bend
1357	–	C–H rock vibrations
1300	–	C–H wag
944	–	= C–H bend
574	559	Metal–nitrogen stretch

due to the existence of BaO groups. Altogether FTIR and Raman studies confirm the molecular structure of the title compound.

3.4 Field emission scanning electron microscopy (FE-SEM) and EDAX studies

FE-SEM investigates the nature and morphology of the crystal surface and identifies the macro and micro blows, porosity of grains, and random crystalline orientation [39, 40]. The grown crystal surfaces have been visualized out by HITACHI S4800 instrument, and the micro-images have been taken with different magnifications. Figure 6a shows the grown crystal surface for 2 μm. Figure 6b, c, d displays the higher magnifications 5 μm, 10 μm, and 20 μm which indicates the presence of small voids and its random distributions over the crystal surface. All the image reveals
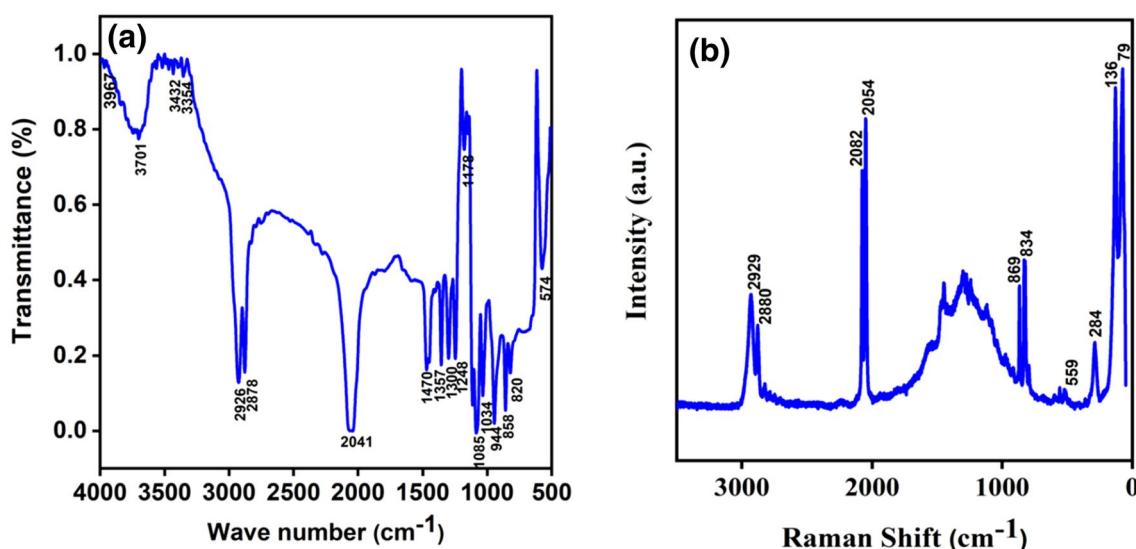

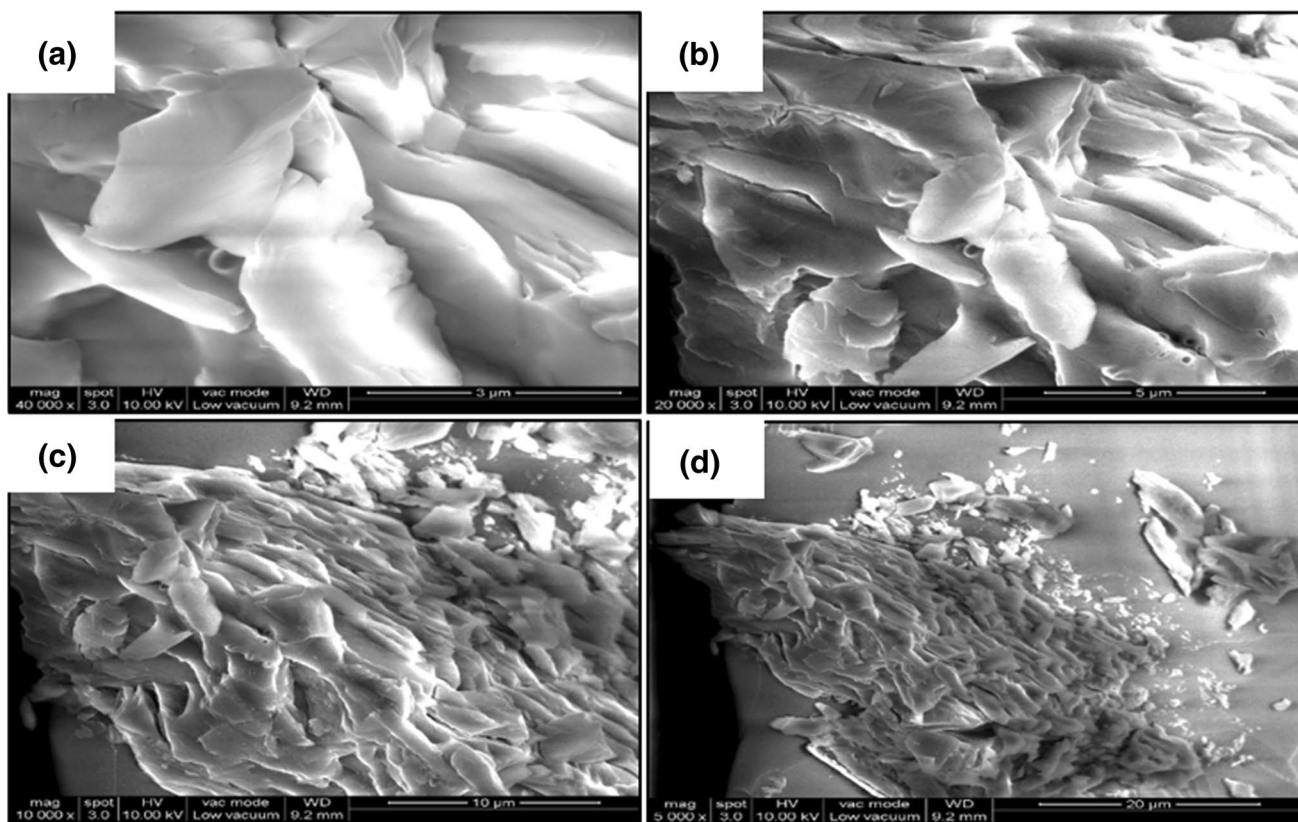**Fig. 5** **a** FTIR spectrum of BBCMTC. **b** Micro-Raman spectrum of BBCMTC

Fig. 6 FE-SEM Micrograph images for BBCMTC single crystal at various magnifications

the grown crystal has defined shape. Additionally, the elemental composition of the grown title crystal was confirmed by EDAX analysis. In Fig. 7, all the fundamental elements like barium (Ba), manganese (Mn), chlorine (Cl), along with other elements of thiocyanate ligand (SCN) like sulphur (S), carbon (C), and nitrogen (N) were identified. The experimental values well-matched to the theoretical values of elemental composition and are listed in Table 5.
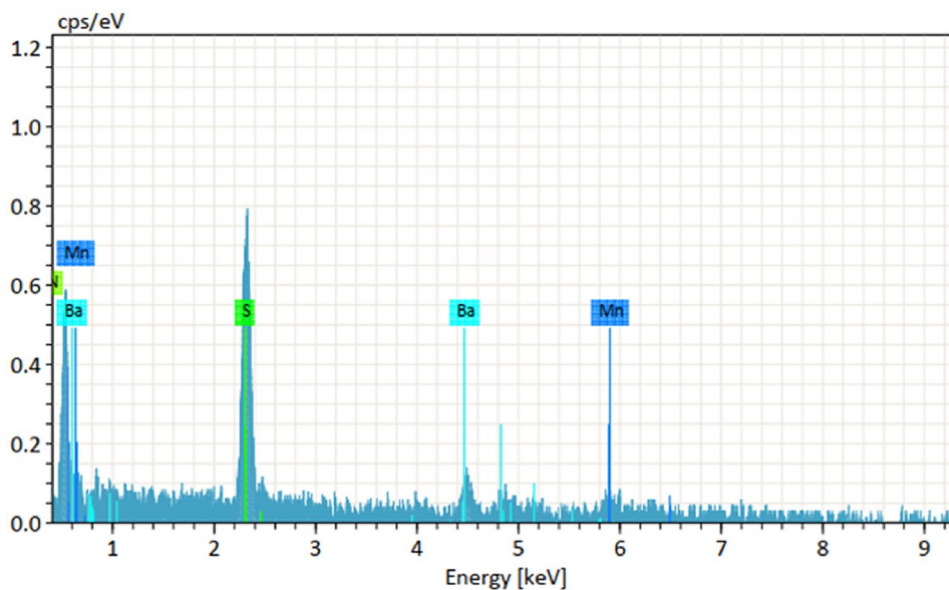
Fig. 7 EDAX Spectrum for BBCMTC

Table 5 The important elemental composition of BBCMTC

Element	At.No	Mass [%]	Atom [%]
C	6	32.34	73.99
S	16	16.39	14.05
Ba	56	14.74	2.95
Mn	25	5.53	2.77
N	7	3.18	6.25
Total	72.18	100	

3.5 Chemical etching studies

The structural information and reverse growth rate on the grown crystal surface can be visualized through the chemical etching studies. Solution growth methods suffer from imperfections like solvent inclusion, grain boundaries, twins, and dislocation [22, 41]. An optical microscope (Olympus) was used to be analyze the surface morphology of BBC-MTC single crystal. The mixed solvent water, ethanol, and methanol with a concentration ratio of 2:2:1 was used as an etchant. Figure 8a shows the crystal surface without etching, and Fig. 8b shows the 15 s etching which has rectangular rock shape pattern. After etching time increase from 15 to 30 s, rock shape layer growth was observed (Fig. 8c) on the crystal surface. The etch pit density (EPD) was estimated using the formula [42].

$$\text{Etch pit density} = \frac{\text{No. of etch pit}}{\text{Area}} \qquad (4)$$

Etching is an essential tool for observing imperfections in the grown crystals. In most cases, defect-free single crystals are necessary for NLO applications. The surface quality and dislocation structure are the most important factors in harmonic generation efficiency (SHG and THG), laser induced damage threshold, mechanical and thermal stability,

etc. The calculated etch pit density (BBCMTC) is 125 cm^{-2}, which is better than the organometallic CMTC single crystal 103 cm^{-2} [49]. It is clear that crystal has good crystalline perfection with less defect and therefore the grown crystal can be utilized in fabrication of NLO devices.

3.6 Vickers's hardness studies

The mechanical behavior of material such as elastic constants, yield strength, brittleness index, and stiffness constant, which indicates whether the crystal belongs to soft or hard material category has been determined by hardness test [43, 44]. Economet VH-1MD hardness tester attached to Vickers's pyramidal indenter was used and the applied loads was varied between 10 and 100 g with a well period of 10 s for all loads. The indented impression of the title compound was seen in the microscope, and the crack occurred on the crystal surface at 100 g. Vicker's hardness number (H_v) of the material was calculated using the standard formula [45]

$$H_v = 1.854 \frac{P}{d^2} \left(\frac{\text{Kg}}{\text{mm}^2} \right) \qquad (5)$$

where H_v is Vicker's hardness number in kg/mm^2, the load applied (P) in kg, and d is the average diagonal length (mm). Figure 9a drawn between H_v versus load P specifies hardness decreases as load increases. Moreover, plot of log (P) versus log (d) shown in Fig. 9b, is in agreement with straight-line slope method and the Mayer's index number (n) was calculated as 3 which shows the title crystal belongs to soft material. Other variation of mechanical properties like yield strength and stiffness constant are displayed in Fig. 9c, d. The grown (BBCMTC) crystal shows good stability compared to the other thiocyanate family crystals such as MCCTC, TMTM and CMCT [3, 46, 47]. Estimated hardness
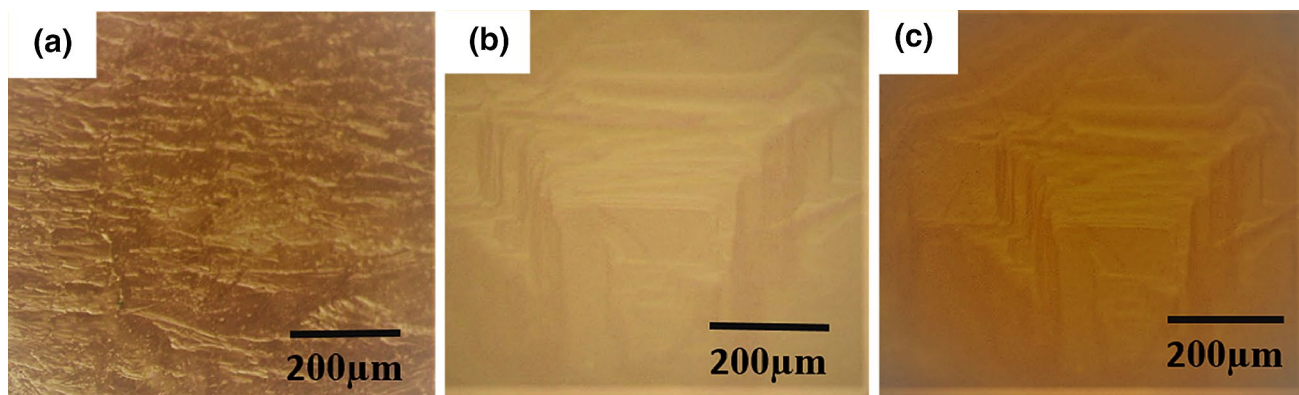

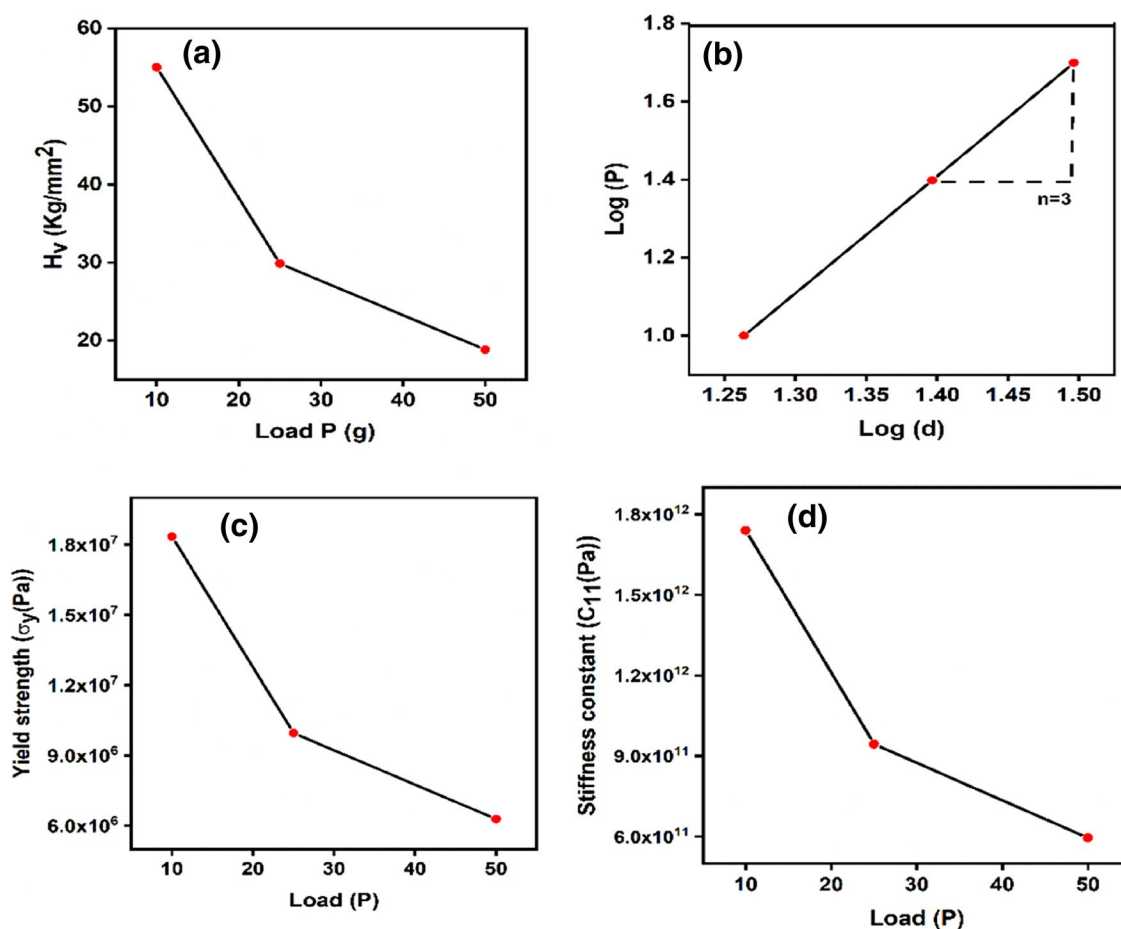**Fig. 8** **a** Before etching, **b** After etching 10 s, and **c** After etching 30 s for BBCMTC single crystal

Fig. 9 **a** Vickers hardness (H_v) versus Load (P). **b** Log (P) versus Log (d). **c** Yield strength (σ_y) versus Load (P). **d** Stiffness constant (C_{11}) versus Load (P)

Table 6 Various thiocyanate family Vickers hardness values of BBCMTC single crystal

Crystal name	VHN in kg/mm^2	Mayer's number	Reference
MCCTC	93.58	1.70	[46]
TMTM	18.6	3.07	[3]
CMCT	--	2.04	[47]
BBCMTC	55.03	3	Present work

parameters compared to the other thiocyanate family are listed in Table 6.

3.7 Thermal analysis

Investigation on the thermal properties of the materials such as phase transition, various stages of decomposition, and higher thermal stability of the material is required for finding the suitability of a material for laser application [48, 49]. The thermal analysis of title compound was performed by TG-DSC thermal analyzer NETZSCH STA 449F3 at a heating rate of 10 °C/min in the nitrogen atmosphere between room temperature and 1400 °C. Figure 10 shows the TG-DSC of the grown crystal. In the TG image, there is no weight loss between 34 and 339 °C, and the title compound is stable up to 339 °C. Nearly 60% of weight loss occur at 382 °C and it corresponds to the decomposition temperature of the material. Moreover, the DSC curve exposes two endothermic peaks at 382 °C and 964 °C and it corresponds to the decomposition temperature of the material. These results show that both TG-DSC trace confirms the decomposition temperature as 382 °C. The thermal stability of BBCMTC is better than other thiocyanate complex crystals like ZCTC (350 °C), MFCTC (234.31 °C), CMTD (150 °C) and BDBCTC (352 °C) [10, 50–52].

3.8 Dielectric studies of BBCMTC crystal

Dielectric materials are insulators, and the solid materials' dielectric behavior is widely applicable for optoelectronic
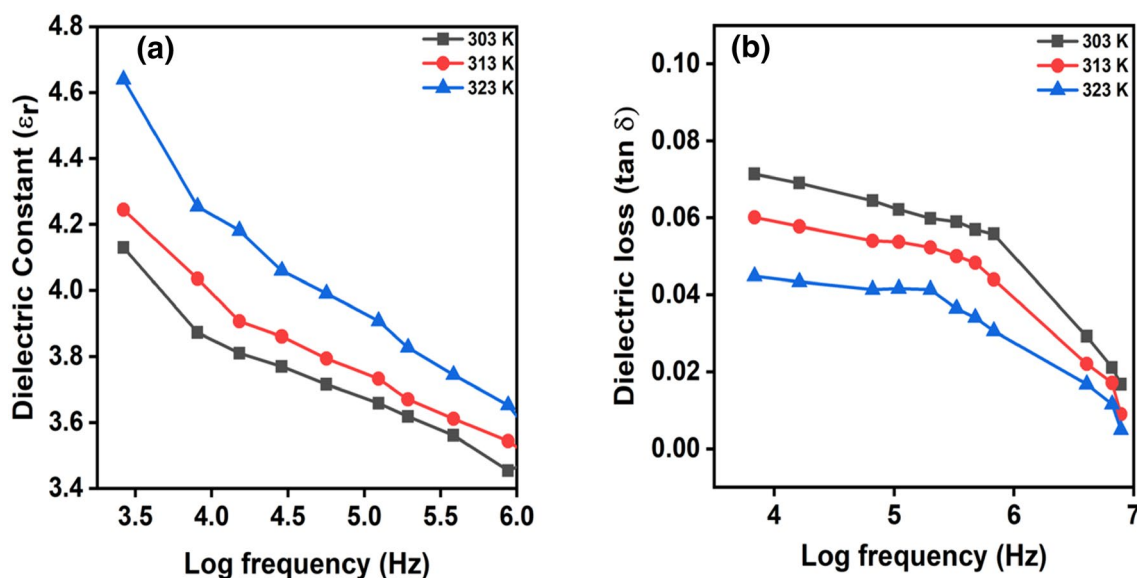
Fig. 10 **a** Dielectric constant (ε_r) versus Log frequency (Hz). **b**. Dielectric loss (taniδ) of BBCMTC versus Log frequency (Hz)

applications [53]. The dielectric measurement of the title compound was carried out by HIOKI 3532–50 LCR meters with different temperatures (303 K, 313 K, and 323 K) at different frequency range from 3 to 7 MHz. The dielectric constant (ε_r) of the BBCMTC crystal was defined using relationship [54].

$$\varepsilon_r = \frac{C_P d}{\varepsilon_0 A} \tag{6}$$

where C_p, A, d, ε_0, are capacitance (in Farad), area of the cross section of crystal (in cm), the thickness of the sample (in mm), and permittivity (8.854×10^{-12} F/m). The material's dielectric constant essentially contributes to polarization like electronic, ionic, orientation, and space charge depending on frequencies [55]. Figure 11a shows the dielectric constant with log frequency at different temperatures; it has observed a higher dielectric constant in the lower frequency region. It arises due to the presence of space charge polarization, which indicates the sample is in perfect crystalline form. Figure 11b shows the dielectric loss with log frequency at various temperatures, which exhibit the low value of tan δ, suggesting the grown crystals have minor defects.

3.9 Dielectric solid-state parameters

The various fundamental factors (SSP) such as valence electron plasma energy ($\hbar\,\omega_P$), Penn gap (E_P), Fermi energy (E_F) and electronic polarizability (α) depends on dielectric constant and can be calculated with standard theoretical calculation as given below.
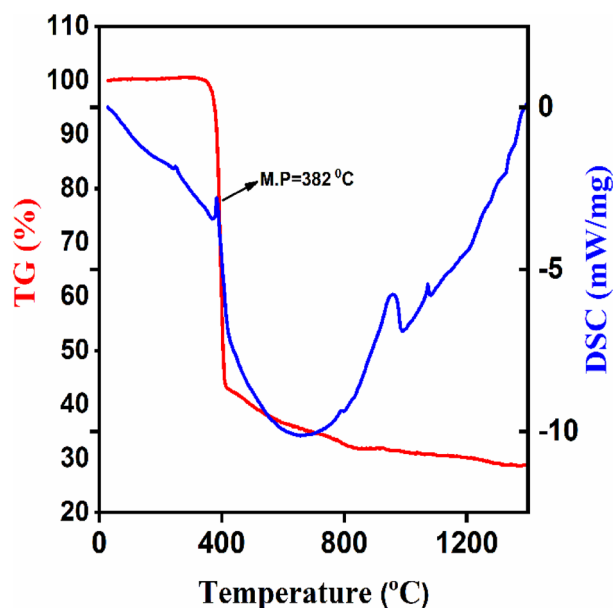

Fig. 11 TG-DSC profile of BBCMTC

The density (ρ) of BBCMTC is determined using the following equation [56]

$$\rho = \frac{MZ}{N_A V} \tag{7}$$

$M = 865.12$ g/mol is the molecular weight ($C_{10}H_{20}O_5$) and unit cell ($Z = 4$), Avogadro's number (N_A) is 6.023×10^{23} mol^{-1} and the unit cell volume (V) is

3692.6 Å. The estimated BBCMTC crystal density (ρ) to be 1.556 g/cm^3. The ($\hbar \omega_P$) is given by [57]

$$\hbar\omega_P = 28.8\left(\frac{Z' \times \rho}{M}\right)^{\frac{1}{2}} \tag{8}$$

where $Z' = [(24 \times Z'_C) + (40 \times Z'_H) + (1 \times Z'_{Ba}) + (1 \times Z'_{Mn}) + (4 \times Z'_N) + (10 \times Z'_O) + (4 \times Z'_S) = 249$ is the total number of valence electrons present in BBCMTC crystal. Here, the valence electron substitution for each C(4), H(1), Ba(2), Mn(7), N(5), O(6) and S(6) was taken with dielectric constant (ε') at 1 MHz for different temperatures (35 °C, 45 °C and 55 °C).

The Penn model, E_P and E_F were evaluated using the relationships [58, 59]

$$E_p = \frac{\hbar\omega_P}{(\varepsilon' - 1)^{\frac{1}{2}}} \tag{9}$$

$$E_F = 0.2948\left(\hbar\omega_P\right)^{\frac{4}{3}} \tag{10}$$

The electronic polarizability (α) of BBCMTC crystal was estimated using the equation [60]

$$\alpha = \left[\frac{\left(\hbar\omega_P\right)^2 S_0}{\left(\hbar\omega_P\right)^2 S_0 + 3E_P^2}\right] \times \frac{M}{\rho} \times 0.396 \times 10^{-24}\text{cm}^3 \tag{11}$$

$$S_0 = 1 - \left[\frac{E_P}{4E_F}\right] + \frac{1}{3}\left[\frac{E_P}{4E_F}\right]^2 \tag{12}$$

where S_0 is constant, Using Clausius Mossotti relation, the value α is derived from the equation [61]

$$\alpha = \frac{3M}{4\pi N_A\rho}\left(\frac{\varepsilon' - 1}{\varepsilon' + 2}\right) \tag{13}$$

Optical band gap (E_g) can be used to define the electronic polarizability (α)

$$\alpha = \left[1 - \frac{\sqrt{E_g}}{4.06}\right]\left[\frac{M}{\rho}\right]0.396 \times 10^{-24}\text{cm}^3 \tag{14}$$

Also with coupled dipole method (CDM) the electronic polarizability (α) title crystal were determined using relation [62]

$$\alpha = \frac{Z'e^2}{m_\rho\omega_0^2} \tag{15}$$

where Z' are the total number of valance electrons, charge of electron ($e = 1.602 \times 10^{-19}$ C), electron mass ($m_e = 9.1 \times 10^{-28}$ g) and 'ω_0' is the natural frequency ($2\pi f_0$), here f_0 is equal to 1 MHz. The fundamental parameters (Penn analysis and Clausius–Mossotti equation) of BBCMTC crystal are much higher compared to MMTG and is summarized in Table 7 [63].

3.10 Z-scan technique

The second-order nonlinear optical susceptibility (χ^2) of BBCMTC is zero because SXRD data collection reveals material crystallized in a centrosymmetric space group with an orthorhombic crystal system [64, 65]. So the third-order NLO coefficients of the material was investigated. Z-scan experimental setup consists of a CW laser with wavelength of 785 nm having power output of 50 mW. The test sample (thickness 1 mm) was mounted on sample container, and the laser beam was focused on it with a convex lens of focal length 10 cm to produce the beam waist ω_0 ($= 2f\lambda/\pi d$) of 5 μm [66]. The focused laser beam passed through a crystal surface, and the resulting transmittance intensity beam was collected using a photodetector and digital power meter. Rayleigh length (Z_R) can be determined using the formula

$$Z_R = \frac{\pi\omega_0^2}{\lambda} \tag{16}$$

The observed Rayleigh range was 0.10 mm [67, 68]. The parameters nonlinear refractive index (n_2) and nonlinear

Table 7 Solid-State parameter of BBCMTC single crystal

SSP-Parameters	'α' values of BBCMTC crystal			MMTG
	35 °C	45 °C	55 °C	
Plasma energy ($\hbar\omega_p$)	19.273 eV	19.273 eV	19.273 eV	6.382
Penn gap energy (E_P)	0.6282 eV	0.9721 eV	0.8680 eV	1.625
Fermi energy (E_F)	15.218 eV	15.218 eV	15.218 eV	34.60
Electronic polarizability (α) using Penn analysis	21.843×10^{-23}cm^3	21.847×10^{-23}cm^3	21.882×10^{-23}cm^3	5.630×10^{-23}cm^3
Electronic polarizability (α) with Clausius–Mossotti equation	21.754×10^{-23}cm^3	21.783×10^{-23}cm^3	21.816×10^{-23}cm^3	5.584×10^{-23}cm^3
Electronic polarizability (α) with Optical band gap	10.730×10^{-23}cm^3	10.730×10^{-23}cm^3	10.730×10^{-23}cm^3	–
Electronic polarizability (α) with CDM	15.926×10^{-23}cm^3	15.926×10^{-23}cm^3	15.926×10^{-23}cm^3	–

absorption coefficient (β) can be determined from the closed and open aperture curve that is displayed in Fig. 12a, b. From the pattern, it is observed that BBCMTC exhibit saturable absorption and self-focusing nonlinearity.

The normalized peak to valley transmittance difference is ΔT_{P-V}, S is linear aperture transmittance that can be expressed as on axis phase shift ($\Delta\Phi$) about the focus using relationships [69]

$$\Delta\Phi = \frac{\Delta T_{P-V}}{0.406(1-S)^{0.25}} \tag{17}$$

$$S = 1 - \exp\left(\frac{-2r_a^2}{\omega_a^2}\right) \tag{18}$$

where the radius of the aperture (r_a) is 3 mm, ω_a are aperture beam radius (0.5 cm) and the calculated S value is 0.5 for the on-axis phase shift ($\Delta\Phi$) value of 0.3954.

Nonlinear third-order refractive index (n_2) and absorption coefficient (β) were calculated using relations [70]

$$n_2 = \frac{\Delta\Phi}{KI_0L_{eff}}\left(\frac{m^2}{w}\right) \tag{19}$$

$$\beta = \frac{2\sqrt{2}\,\Delta T}{I_0 L_{eff}}\left(\frac{m}{w}\right) \tag{20}$$

where K is wave vector ($2\pi/\lambda$) and laser beam intensity (I_0), ΔT, L_{eff} is open aperture peak value at Z-scan and effective sample thickness which was determined using the relationship

$$L_{eff} = \frac{1 - \exp(-\alpha L)}{\alpha} \tag{21}$$

where the linear absorption coefficient is α, sample thickness is L (= 1 mm). The real and imaginary third-order NLO susceptibility (χ^3) parts are calculated using the standard relations [71]

$$R_e(\chi^3) = \frac{10^{-4}\varepsilon_0 C^2 n_0^2 n_2}{\pi}\left(\frac{cm^2}{w}\right) \tag{22}$$

$$I_m(\chi^3) = \frac{10^{-2}\varepsilon_0 C^2 n_0^2 n_2^2 \lambda \beta}{4\pi^2}\left(\frac{cm}{w}\right) \tag{23}$$

where permittivity (ε_0) is 8.854×10^{-12} F/m, velocity of light in vacuum ($C = 3 \times 10^8$ m/s) and n_0 are sample linear refractive index at 785 nm.

The third-order nonlinear optical susceptibility of BBCMTC crystal was determined by adding real and imaginary (χ^3) parts as [51]

$$\left|\chi^{(3)}\right| = \sqrt{\left(R_e(\chi^3)\right)^2 + (I_m(\chi^3))^2} \tag{24}$$

The determination of second-order hyper polarizability of BBCMTC (γ) was associated with third-order NLO susceptibility [72]

$$\gamma = \frac{\chi^{(3)}}{N^* f^4} \tag{25}$$

$$N^* = \frac{\rho N_A}{M} \tag{26}$$

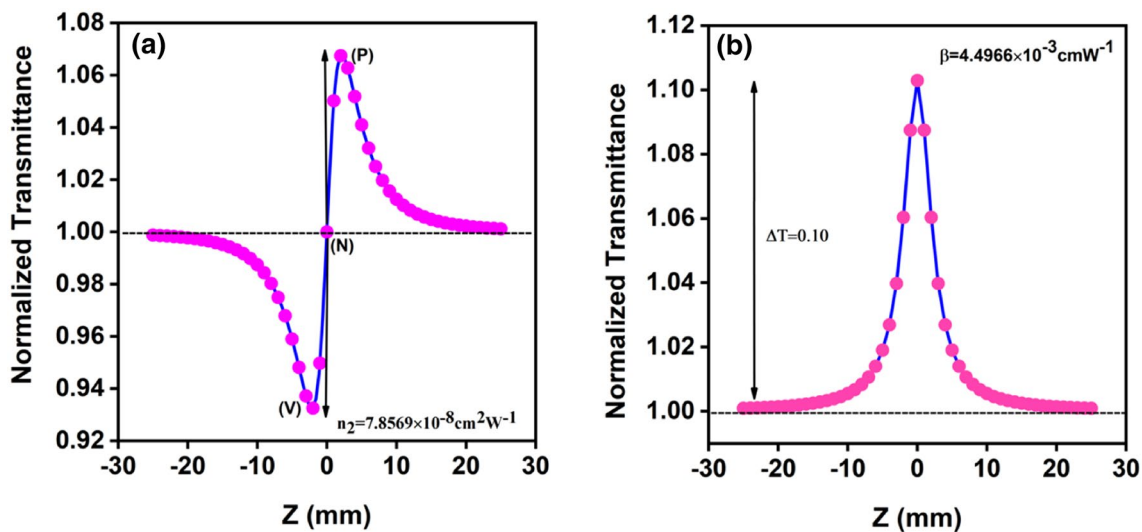**Fig. 12 a** Closed aperture Z-scan patterns of BBCMTC single crystal. **b** Open aperture Z-scan patterns of BBCMTC single crystal

where N^* is a number of molecules per unit volume, ρ is crystal density, N_A is Avogadro's number and the molecular weight of the sample are M.

The correction factor for the local field (f) was determined using the Lorentz equation

$$f = \frac{(n_0^2 + 2)}{3} \tag{27}$$

The ratio of real and imaginary part of third-order susceptibility (χ^3) known as coupling factor (ρ^*) is

$$\rho^* = \frac{I_m(\chi^3)}{R_e(\chi^3)} \tag{28}$$

The estimated nonlinear third-order optical parameters are n_2 is $7.85 \times 10^{-8} cm^2 w^{-1}$ and β is $4.49 \times 10^{-3} cmw^{-1}$. The third-order susceptibility (χ^3) of organometallic thiocyanate crystal is found to 11.55×10^{-5} esu and the calculated second-order hyper polarizability molecules (γ) value is 5.28×10^{-26} esu. The BBCMTC third-order NLO susceptibility values are higher compared to other thiocyanate crystals and the values are listed in Table 8 [33, 49]. The low-energy d-d transition interact with π-electron delocalization system due to increased charge transfer are responsible for higher (χ^3) and polarizability (γ). These organometallic complexes can be used for frequency tripling and optical switching applications [73].

4 Conclusion

Single crystals of BBCMTC with dimensions of $10 \times 5 \times 2$ mm^3 was grown by SEST at ambient temperature. The title compound crystallizes in the orthorhombic system with space group Pnma. The lattice cell parameters of the title compound was evaluated as $a = 15.9102$ Å, $b = 12.6164$ Å, $c = 18.3959$ Å and $V = 3696.26$ Å^3. The crystal possess lower cut-off wavelength of 287 nm with bandgap energy of 4.1 eV. The C–N stretching molecular vibrations of thiocyanate group, metal–nitrogen vibration and Ba–O vibrations were identified in the FTIR and micro-Raman analysis. SEM analysis and Etch pit pattern indicate the presence of small voids and its random distributions over the crystal surface. The grown (BBCMTC) crystal shows good stability compared to the other thiocyanate family crystals such as MCCTC, TMTM and CMCT. Both TG-DSC trace confirms the decomposition temperature as 382 °C. The dielectric constant and loss has a higher value in the low frequency region and a lower value in high frequency region due to the contribution of space charge polarizations. The SSP factors such as Valence electron plasma energy ($\hbar \omega_P$), Penn gap (E_P), Fermi energy (E_F) and electronic polarizability (α) were calculated. BBC-MTC exhibit saturable absorption and self-focusing nonlinearity. The BBCMTC third-order NLO susceptibility values are higher compared to other thiocyanate

Table 8 Z-scan measurement details and the various parameters of the BBCMTC single crystal

Z-Scan parameters	BBCMTC (present work)	MMCTC	MMTC
Laser type	Continuous wave laser	Infrared laser beam	He–Ne laser
Wavelength of the input laser	785 nm	632 nm	632 nm
Lens focal length	10 cm	3.3 cm	–
Diameter of the laser beam	0.1 cm	–	–
Sample thickness	0.1 cm	3.3 mm	–
Aperture radius	3 mm	2 mm	–
Intensity of the laser	1.784 KW/cm^2	26.5	–
Optical path distance	1 mm	85 cm	–
Beam waist (ω_0)	5 μm	–	–
Rayleigh length (Z_R)	0.10 mm	1.98 mm	–
Effective thickness (L_{eff})	0.98 mm	–	–
Nonlinear refractive index (n_2)	7.85×10^{-8} cm^2/w	8.57×10^{-13} cm^2/w	-1.08×10^{-12} cm^2/w
Nonlinear absorption coefficient (β)	4.49×10^{-3} cm/w	8.14×10^{-6} cm/w	8.65×10^{-6} cm/w
Real part of the third-order susceptibility [$R_e(\chi^3)$]	31.42×10^{-7} cm^2/w	5.22×10^{-11} cm^2/w	2.61×10^{-9} cm^2/w
Imaginary part of the third-order susceptibility [$I_m(\chi^3)$]	11.24×10^{-5} cm/w	2.49×10^{-9} cm/w	6.04×10^{-9} cm/w
Third-order nonlinear optical susceptibility (χ^3)	**11.55×10^{-5} esu**	11.22×10^{-37} esu	3.13×10^{-8} esu
Second-order molecular hyper polarizability (γ)	5.28×10^{-26} esu	–	–
Number of molecules per cm^3 (N^*)	$1.08 \times 10^{+21}$ cm^3	–	–
Coupling factor (ρ^*)	0.35	–	–

Boldface indicates that the third-order nonlinear susceptibility of the grown BBCMTC crystal is greater than those of other thiocyanate crystals [MMCTC, MMTC]

crystals. Thus, organometallic complexes like BBCMTC can be used for frequency tripling and optical switching applications.

References

1. P. Sakthi, R. Rajasekaran, D. Balasubramanian, J. Adv. Phys. **5**, 199–206 (2016)
2. K.S. Kumat, A. Baskaran, V. Ramesh, S. Murugavel, P. Sagayaraj, K. Rajarajan, Opt-Int. J. Light Electron Opt. (2016)
3. G. Pabitha, R. Dhanasekaran, Mater Sci. Eng. B **177**, 1149–1155 (2012)
4. T.A. Hegde, A. Dutta, V. Gandhiraj, Int J Eng Technol. Innov. **9**(4), 257 (2019)
5. X.Q. Wang, D. Xu, M.K. Lu, D.R. Yuan, S.X. Xu, Mater. Res. Bull. **36**(5–6), 879–887 (2001). https://doi.org/10.1016/S0025-5408(01)00573-6
6. X.Q. Wang, D. Xu, M.K. Lu, D.R. Yuan, S.X. Xu, S.Y. Guo, G.H. Zhang, J.R. Liu, J. Cryst. Growth **224**(3–4), 284–93 (2001)
7. D. Yuan, D. Xu, M. Liu, F. Qi, W. Yu, W. Hou, Y. Bing, S. Sun, M. Jiang, Appl. Phys. Lett. **70**(5), 544–546 (1997)
8. R.J. Usha, P. Sagayaraj, V. Joseph, Spectrochim. Acta part A Mol. Biomol. Spectrosc. **133**, 241–249 (2014). https://doi.org/10.1016/j.saa.2014.04.161
9. P.N. Kumari, S. Kalainathan, N.A. Raj, Mater. Res. Bull. **42**(12), 2099–2106 (2007)
10. V. Ramesh, A.S. Syed, K. Jagannathan, K. Rajarajan, Spectrochim. Acta Part A: Mol. Biomol. Spectrosc. **108**, 236–243 (2013)
11. S. Cynthia, S. Sagadevan, L. Mariappan, J. Mater. Sci.: Mater. Electron **28**, 14787–14797 (2017)
12. R.D. Shannon, Acta Cryst. **A32**, 751–767 (1976)
13. K. Rajarajan, K.S. Kumar, J. Therm. Anal. Calorim **112**, 1297–1302 (2013)
14. R. Vukovic, A. Erceg, V. Pillizota, D. Ubaric, Acta Aliment. **28**(2), 141–147 (1999)
15. A.M. Arif, A. Yousaf, H.-L. Xu, Z.-M. Su, J. Mol. Liq. **301**, 112492 (2020)
16. S-L Li, J-Y Wu, Y-P Tian, H Ming, P Wang, M-H Jiang, H-K Fun, https://doi.org/10.1002/ejic.200500906
17. Bruker APEX2 and SAINT. Bruker AXS Inc., Madison, Wisconsin, USA (2008)
18. G.M. Sheldrick, *SADABS Program for Area Detector Absorption Correction* (University of Gottingen, Germany, 1996)
19. A short history of SHELX, G. M. Sheldrick, Acta Cryst. **A64**, 112–122 (2008)
20. X.Q. Wang et al., J. Cryst. Growth **224**, 284–293 (2001)
21. X.Q. Wang et al., Phys. Stat. Sol. (a) **191**, 106–116 (2002)
22. X.Q. Wanget, Phys. B: Condens. Matter **405**, 1071–1080 (2010)
23. C.M. Raghavan, A. Bhaskaran, R. Sankar, R. Jayavel, Curr. Appl. Phys. **10**, 479–483 (2010)
24. G.M. Sheldrick, Acta Cryst. **C71**, 3–8 (2015)
25. C. Zhiqiang, L. Kai, N. Meiju, W. Daqi, Acta Cryst. **E66**, m68 (2010)
26. V. Ramesh, K. Rajarajan, B. Gunasekaran, IUCrData **4**, x190888 (2019)
27. V. Ravisankar, V. Ramesh, M. Krishnamohan, B. Gunasekarana, T.C.S. Girisun, IUCrData **6**, x210024 (2021)
28. M. Packiyaraja, S.M. RaviKumar, R. Srineevasan, R. Ravisankar, Mater. Sci. Eng. **360**(1), 012031 (2018). https://doi.org/10.1088/1757899X/360/1/01203
29. R. Sankar, C.M. Ragavan, M. Balaji, R. Mohankumar, R. Jayavel, Cryst. Growth Des. Mater. Sci. Eng. **3600120317**, 348 (2007)
30. X.Q. Wangetal, Mater. Res. Bull. **36**, 1287–1299 (2001)
31. K. Rajarajan et al., Mater. Manuf. Processes **22**, 370–374 (2007)
32. P.N.S. Kumari, S. Kalainathan, N.A.N. Raj, Mater. Res. Bull. **42**, 2099–2106 (2007)
33. V. Ramesh, B. Gunasekaran, M. Krishnamohan, K. Rajarajan, Mater. Res. Expr. **6**, 116205 (2019)
34. R. Robert, C.J. Raj, S. Krishnan, S.J. Das, Phys. B **405**, 20–24 (2010)
35. H. Yang, L. Jun, B. Han, S. Zhenjia, W. Ming, Z. Zhongxiang, J. Adv. Ceram. **9**(5), 641–646 (2020). https://doi.org/10.1007/s40145-020-0398-1
36. H.B. Han, L. Jun, H. Yang, Z. Zhongxiang, J. Adv. Ceram. **9**(4), 511–516 (2020). https://doi.org/10.1007/s40145-020-0384-7
37. B. Han, L. Jun, H. Yang, X. Tongtong, Z. Zhongxiang, Appl. Phys. Lett. **117**(4), 042904 (2020). https://doi.org/10.1063/5.0016342
38. J. Li, Xu. Tongtong, L. Liu, Y. Hong, Z. Song, H. Bai, Z. Zhou, Ceram. Int. **47**, 19247–19253 (2021)
39. A.H. Tejaswi, D. Atanu, G. Vinitha, Int. J. Eng. Tech. Innov. **9**(4), 257–286 (2019)
40. P. Paramasivam, C.R. Raja, Spe Chim. Acta Part **A79**, 1109–111 (2011)
41. S. Gunasekaran, S. Ponnusamy, Cryst. Res. Technol. **41**, 130 (2006)
42. C. Topacli, A. Topacli, J. Mol. Struct. **644**, 145 (2003)
43. C.M. Raghavan, R. Sankar, R. Mohankumar, R. Jayavel, J. Cryst. Growth **311**, 1346–1351 (2009)
44. C. Muthuselvi, B. Sumathi, B. Ravikumar, Pharm. Chem. J. **5**(5), 35–45 (2018)
45. J. Arumugam, M. Selvapandiyan, C. Senthilkumar, M. Srinivasan, P. Ramasamy, J. Mater. Sci: Mater. Electron. (2020). https://doi.org/10.1007/s10854-020-03161-9
46. S. RafiAhamed, J. Balaji, P. Srinivasan, Mater. Res. Innov. (2017). https://doi.org/10.1080/14328917.2017.1320837
47. V. Ravisankar, V. Ramesh, B. Gunasekaran, M. Krishnamohan, T.C.S. Girisun, A. Dhanusha, ECS J. Solid State Sci. Tech. **10**, 091008 (2021). https://doi.org/10.1149/2162-8777/ac2325
48. V. Ramesh, B. Gunasekaran, P. Suresh, E. Sundaravadivel, K. Showrilu, K. Rajarajan, IOP Conf. Ser.: Mater. Sci. Eng. **872**, 012175 (2020)
49. T.A. Hegde, A. Dutta, G. Vinitha, Appl. Phys. A **124**, 808 (2018)
50. C. Balarew, R. Duhlew, J. Solid State Chem. **551**, 1–6 (1984)
51. N.M. Ravindra, V.K. Srivastava, J. Infrared Phys. **20**, 67–69 (1980)
52. X.Q. Wang et al., Opt. Mater. **23**, 335–341 (2003)
53. C.M. Raghavan, R. Sankar, R.M. Kumar, R. Jayavel, J. Cryst. Growth **310**, 4570–4575 (2008)
54. R. Hanumantharao, S.K. Hindawi, Corp. J. Chem. (2013). https://doi.org/10.1122/2013/305932
55. K. Sangwal, Mater. Chem. Phys. **63**, 145–152 (2000)
56. R. Vivekanandhan, K. Raju, S.S.J. Dhas, V. Chithambaram, Int. J. App. Eng. Res. **13**(18), 13454–13459 (2018)
57. N. Saravanan, V. Chithambaram, V. Ravisankar, J. Mater. Sci: Mater. Electron. **29**, 5009–5013 (2018)
58. E.M. Onitsch, Systematic metallographic and mineralogic structures. Mikroscopia **2**, 131–151 (1947)
59. M. Meena, C.K. Mahadevan, Cryst. Res. Technol. 43166 (2008)
60. R.C. Miller, Appl. Phys. Lett. **5**, 17 (1964)

61. P. Rekha, G. Chakkaravarthi, R.M. Kumar, G. Vinitha, R. Kanaga-durai, J. Mater. Sci.: Mater. Electron. (2019). https://doi.org/10.1007/s10854-019-01279-z
62. J.D.Jackson, ClassicalElectrodynamics, WileyEastern.321 (1978).
63. D.R. Penn, Phys. Rev. **128**, 2093–2097 (1962)
64. C. Sundararaja, S. Sagadevan, Mater. Res. **21**(1), e20160595 (2018)
65. P.V. Rysselberghe, J. Phys. Chem. **36**, 1152–1155 (1932)
66. M.J. Renne, B.R.A. Nijboer, Chem. Phys. Lett. **1**, 317 (1967)
67. B.R.A. Nijboer, M.J. Renne, Chem. Phys. Lett. **2**, 35 (1968)
68. B.W. Kwaadgras, M. Verdult, M. Dijkstra, R. van Roij, J. Chem. Phys **135**, 134105 (2011)
69. R. Anbarasan, M.A. Lakshmi, J.K. Sundar, J. Mater. Sci.: Mater. Electron. **29**, 14827–14834 (2018)
70. R. Dhanjayan, S. Gunasekaran, S. Srinivasan, Mater. Lett. **206**, 221–224 (2017). https://doi.org/10.1016/j.matlet.2017.07.028
71. S.N. Jayanthi, N. Bhuvaneswari, Mater. Today: Proc. **5**, 3361–3368 (2018)
72. M. Sheik-Bahae, A.J. Said, Quantum. Electron **26**, 760–769 (1990)
73. N.Y. Kamber, G. Zhang, S. Liu, S.M. Mikha, W. Haidong, Opt. Commun **184**, 475–483 (2000)

Publisher's Note Springer Nature remains neutral with regard to jurisdictional claims in published maps and institutional affiliations.